[SSC20-WP1-02]

Towards the Use of Commercial-off-the-Shelf Small-Satellite Components for Deep-Space CubeSats: a Feasibility and Performance Analysis

Stefano Casini
Hyperion Technologies BV and Delft University of Technology
Vlinderweg 2, 2623 AX Delft, The Netherlands, +31 (0)15-5160905
s.casini@tudelft.nl

Iosto Fodde, Steven Engelen, Bert Monna
Hyperion Technologies BV
Vlinderweg 2, 2623 AX Delft, The Netherlands, +31 (0)15-5160905
i.fodde@hyperiontechnologies.nl

Angelo Cervone, Eberhard Gill
Delft University of Technology
Kluyverweg 1, 2629 HS Delft, The Netherlands, +31 (0)15 27 89804
a.cervone@tudelft.nl

ABSTRACT

The aim of this paper is to assess the feasibility of using currently available commercial-off-the-shelf (COTS) small-satellites components in deep-space scenarios, studying their applicability and performance. To evaluate the performances, an asteroid fly-by mission is briefly introduced, but several of the selection criteria and ideas can be extended to other deep space mission concepts. This particular mission scenario requires to follow three main trends: miniaturization, standardization and automation. For this reason the mission represents a good test bench scenario to analyze the products of the current small-satellites industry. Once the reference mission has been defined, the preliminary ΔV is computed and the micro-propulsion system is selected. Afterwards, for several satellite subsystems the requirements are compared with the expected performance of a set of small-satellite components currently available on the market. Once the most promising hardware solutions are identified, mass and volume budgets are defined. Subsequently, drawbacks and limits of using COTS components for deep-space exploration are highlighted, focusing on the readiness level of each subsystem. Finally, recommendations are given on what methods and hardware are needed in the near future to overcome the limiting factors and to allow deep-space exploration using low-cost CubeSats.

INTRODUCTION

Earth-based CubeSats are currently widely used by both industry and scientific community for various applications. The use of CubeSats beyond Earth orbits has seen less of a rise as these types of missions have stricter requirements and higher costs due to mission-specific hardware, which do not fit the CubeSat philosophy of re-usability and cheap COTS components. However, successfully flown missions (e.g. the MarCO CubeSats[1]) and accepted proposals (e.g. the HERA mission[2]) show a significant interest and desire for these types of missions, as they have the potential of significantly reducing the cost of Solar System exploration. Besides the reduction of mass and size, an increase in autonomy and the use of COTS components are also important factors, as currently most hardware and software are specifically designed for interplanetary missions.

On the other hand, the increasing interest of the space community in asteroids exploration is testified by the large amount of missions planned by the major space agencies[3,4,5]. Some of those mission proposal include the use of CubeSats, but their customized design does not match the CubeSat philosophy that characterized the last couple of decades of Earth's small satellite design. The large number of Near Earth Asteroids[6] (NEAs) and the various applications (scientific exploration, deflection of hazardous objects, in-situ resources mining) suggest a massive exploration of the NEA belt that will characterize the next decades of Solar System exploration. However, the small diameter and the poor

illumination of minor bodies pose several challenges in their close-proximity exploration. For these reasons, asteroids exploration may require a significant change of mindset, that can eventually take advantage of the fast-growing small-satellites COTS components industry[7]. Due to the large amount of minor bodies, a cheap, small, standardized CubeSat architecture can be used to obtain information over a large number of asteroids, identifying interesting targets and enlarging their dataset for future larger and more expensive missions. To overcome the cost obstacle, three main trends should be followed: miniaturization, standardization and automation. The majority of deep-space CubeSats proposed through the years ranges between 6U to 12U [1,2,8,9,10,11]. For this particular application, a more light and compact solution is investigated, trying to obtain a 3U stand-alone CubeSat.

First, an example mission is discussed to allow the generation of a set of requirements for the individual subsystems. As the goal of the paper is to analyze the applicability of COTS components to a general deep space mission, a detailed mission design for a specific target shall not be performed here. Instead, the goals and requirements shall be based on previous missions and research on deep space mission design. Hereafter, payload selection is presented, followed by micro-propulsion system analysis based on simplified trajectory considerations. Afterwards, several other subsystems (navigation, Attitude Determination and Control System (ADCS), communications, On-Board Data Handling (OBDH), power) are presented and evaluated. Finally considerations of the overall architecture are presented, with emphasis on the readiness level of the already available on the market COTS components.

ASTEROID FLY-BY MISSION DEFINITION

This section is intended to briefly introduce the reference mission, used as a test bench for the evaluation of the COTS components. Where necessary, simplified requirements are defined in each specific section.

Several mission concepts have been proposed to explore asteroids, including motherships carrying several CubeSats on-board[3], and stand-alone missions[9]. The missions are based on a rendezvous or a fly-by of the target. The former usually allows a more extensive exploration of the target, but it also requires a significantly larger ΔV, which complicate the design of a small and cheap CubeSat. The latter has a significantly shorter scientific phase, but with a much smaller ΔV. The short scientific phase, in this particular mission scenario, simplifies the design of some subsystems, due to the smaller dataset that has to be transferred to the Earth, which simplifies the design and thus reduces the cost of the mission.

As a reference test case, an asteroid fly-by mission is defined. However, differently from other mission proposals, the spacecraft injection is considered around the Earth, in order to further stress the components evaluation. Besides being a test scenario, this mission is a good representative of the current space exploration trends. Table 1 reports some mission characteristics. As the main focus of this paper is not the design of such a mission, but mostly the component selection, the requirements shall not be as detailed and extensive as is needed for an actual mission.

Table 1:Mission Objectives (MO), Mission Philosophy (MP), Mission Requirements (MR)

Code	Description
MO	Improve Near Earth Asteroids dataset (Dimension, shape, rotational parameters, composition, ephemerides).
MP	Maximize the scientific return with limited cost (COTS components, autonomous GNC, commercial launcher) and size (3U).
MR1	Payload shall observe the asteroid in the visible range.
MR2	Payload shall observe the asteroid in the IR range.
MR3	Target shall have a minimum diameter of 100m to have a sufficient scientific return.

The high-level mission requirements shown in Table 1 are derived from the mission objectives and are used in the sections (especially Payload section) to determine the subsystem requirements components evaluation.

The fly-by altitude will be considered ranging from 300 to 500 km, since it has been proved that a 3U CubeSat, leaving from a Sun-Earth Lagrangian point Halo orbit, is able to fly-by an asteroid with an altitude below 500 km[12].

This paper focuses on a general asteroid fly-by mission, thus a specific target shall not be chosen here. A general list of potential targets is given in the Propulsion section and for specific calculations a representable number is given from that table. Nevertheless, the next sections contain comments on the applicability of certain COTS components for other applications. For example, mothership architecture, close proximity operations and large CubeSat platform applicability will be often mentioned. This is done on purpose to keep track of the main goal of this paper: evaluating COTS components deep-space applicability.

SCIENTIFIC INSTRUMENTS - PAYLOAD

The scientific payload is usually the most customized subsystem for a space mission as it strongly depends on

the mission objectives. Looking at the mission objectives and requirements stated in Table 1, the spacecraft needs to contain a visible camera for physical characteristic, such as shape and dimension, and an IR spectrometer for composition-related studies. Using the mission objectives and requirements, a small representative set of requirements can be generated for the payload selection. Table 4 reports the payload requirements.

Table 4: Payload Requirements

Payload Requirements	Description
PR1 The optical camera (visible) shall provide a minimum resolution of 50 m/pixel at fly-by altitude.	A minimum number of pixels to describe the asteroid shape is required. PR1 enables to describe a 300-m diameter asteroid with approximately 36 pixels.
PR2 The payloads mass shall not exceed 500 g.	As it will be shown in the following sections, the CubeSat total mass should be kept below 4 kg, so a lighter payload is strongly recommended.
PR3 The payloads volume shall not exceed 0.8 U.	The 3U CubeSat should allocate all the necessary subsystems. As it will be shown, the payload needs to be compact.
PR4 The instrument FOVs shall be larger than the ADCS pointing accuracy.	The target should always be in the FOV of the instruments to perform science.

Many COTS CubeSat cameras are available on the market, but only few of them meet the requirements (especially in terms of mass and volume) of this application. A list of several COTS optical cameras is given in Table 5.

Not included in Table 5, Thoth Technology Argus 2000[19] is an IR spectrometer characterized by around 300 g and by 80 mm x 46 mm x 80 mm volume. It has a narrow FOV (0.15º) which makes it suitable for closer applications.

ESA M-ARGO payload will include the Multi-spectral imager ASPECT[9] from VTT, characterized by three acquisition channels (VIR, NIR and SWIR). Even if it is not a COTS instrument, its small volume (1U), mass (950 g) and power consumption (7 W), make it a valid candidate alternative to the COTS camera and spectrometer, especially for larger applications.

Hyperion Technologies IM200 appears as the most promising solution in terms of accuracy, mass and volume configuration. Moreover, its resolution make it suitable to be used also as a NAVCam, as will be further discussed in the Navigation section. For larger CubeSats, where mass and volume requirements would be less strict, SCS Space Gecko Imager represents an excellent alternative in terms of accuracy. If the requirements are even less strict, Simera Sense HyperScape100 and Simera Sense MultiScape100 would ensure an incomparable resolution together with the possibility of performing VIS and NIR measurements with the same instrument.

Table 5: COTS Cameras

COTS Cam.	Mass [g]	Dim .[mm]	Peak Power [mW]	Pixels [MP]	FOV [deg]	GSD @ 300 km [m/pixel]
Hyperion IM200[13]	59	29 x 29 x 70.7	1000	4	~20x 20	~28
Crystal Space Micro Camera System[14]	<50	45 x 25 x 45	240	0.3	44 x 34	~300
XCAM C3D[15]	85	95 x 91 x 27	845	1.3	38 x 31	~165.6
SCS Space Gecko Imager[16]	390	56 x 97 x 96	2700	N/A	N/A	~23.4
Hyper Scout Cosine[17]	1100	~ 100 x 100 x 100	N/A	8	N/A	40
Simera Sense Hyper Scape100[18]	1200	98 x 98 x 176	<6000	4	2.22	~3
Simera Sense MultiScape100[18]	1200	98 x 98 x 176	<6000	4	2.22	~3
Simera Sense TrtiScape100[18]	1100	98 x 98 x 176	<6000	12	2.22	~3

Argus 2000 represents the only off-the-shelf IR spectrometer, and its IR range is smaller than ASPECT's range (1240-2000 nm compared to 900-2500 nm). Moreover, its narrow FOV poses several challenges in a 300-500 km fly-by altitude. Nevertheless, it is the only IR spectrometer able to meet the strict mass and volume requirements.

Laser altimeters are out of the scope of this paper because the market does not offer COTS solution. However, it is not possible to exclude that in the near-future commercial-off-the-shelf laser altimeters will be available on the market. Indeed, laser telecommunication research is growing fast and it is characterizing the small-satellites industry[20,21]. An improvement of the small laser altimeter technology would be highly beneficial for asteroid mission, in order to improve scientific return (topography, gravitation) and to improve relative navigation.

Even though magnetic field analysis is important in close proximity operations rather than high altitude fly-bys, it is important to remember that many magnetometers are available on the market for attitude determination, but clearly they cannot be used for deep-space applications. However, they can be re-converted to be used as a payload, if extra volume and mass is available, due to their really compact and low-power configuration. An example of this is the Hyperion Technologies MM200[22], which with its 20 mm x 20 mm x 11.3 mm volume, 10 g mass and 10 mA peak power consumption, represents an extra payload feasible for this mission architecture.

PROPULSION

The micro-propulsion system is usually the largest and the most demanding in terms of mass and volume, thus it is seen as one of the driving subsystems for this mission. A further cost decrease can be obtained by taking advantage of commercial launches instead of deep-space launches. For this reason an Earth sphere-of-influence (SOI) escape scenario is considered, with the goal of achieving a ballistic transfer able to fly-by (or impact) an asteroid. Earth escape problem has been investigated in previous work and solutions have been proposed: chemical propulsion followed by electric low-thrust trajectory[23], low-thrust escape trajectory[24], micro-propulsion staging[25]. However, all of these solutions consider customized propulsion systems, which is ruled out for this paper to ensure the COTS subsystems constraint.

NASA-JPL Small Body Search Engine[26] has been used to preliminary compute the required Earth's SOI escape velocity, V_{∞}, to inject the spacecraft in an interplanetary ballistic transfer towards the target asteroids. Table 6 gives a short list of targets with their departure dates and required escape velocity.

As injection orbit, a Super Synchronous Geostationary Transfer Orbit (SSGTO) has been selected, due to its high energy and commercial nature, which would further decrease the costs. SSGTO is characterized by apogee and perigee altitudes respectively of 295 km and 90 000 km[23]. Using the patched conics approach, it is possible to compute the approximated ΔV to deliver to the spacecraft at the perigee, and to inject it on an escape hyperbola. Figure 1 shows the relation between the escape velocity V_{∞} and the perigee ΔV.

Table 6: Targets

Name	Departure Date	ToF [days]	V_{∞} [km/s]	Diam. [m]
99942 Apophis	2028-08-26	230	0.1	340
1943 Anteros	2025-12-20	165	0.5	2300
2102 Tantalus	2034-04-27	635	0.5	1650
3200 Phaethon	2028-03-04	985	0.6	300
4034 Vishnu	2033-04-27	510	0.4	420
4660 Nereus	2028-05-18	100	0.2	330
7482	2031-04-08	640	0.4	1052
11500 Tomaiyowit	2035-04-12	235	0.6	738
13651	2029-04-03	815	0.4	562
35107	2025-01-14	205	0.2	929
65679	2036-11-17	615	0.5	918
66391 Moshup	2036-02-01	115	0.3	1317
138127	2027-05-24	260	0.5	754
142464	2034-08-20	625	0.5	886
153201	2032-07-01	535	0.3	510
161989 Cacus	2039-12-17	635	0.2	1900

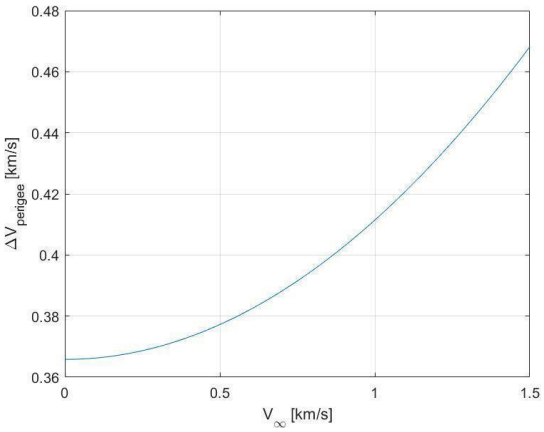

Figure 1: SSGTO required ΔV

On top to the main ΔV , additional ΔVs need to be taken into account to deal with: eventual redirection maneuver out of the SOI, gravitational losses, fly-by correction maneuvers. It is possible to compute the correction

maneuver ΔV to deliver to the spacecraft to redirect it on the correct direction as follows:

$$\Delta V=\sqrt{2V_{\infty}^{2}(1-cos\,(\varphi)\,)} \quad (1)$$

Where φ is the required correction angle at the exit of the SOI. Figure 2 shows the required ΔV in terms of correction angle and escape velocity, showing that for low escape velocity and low correction angles the required ΔV is well below 50 m/s. Usually gravitational losses are around the 10% of the total ΔV[23]. It has been shown that a total of 70 m/s is required to fly-by an asteroid leaving from Earth-Moon L1-L2[27]. The total ΔV is composed by two nominal impulses to leave the Lagrangian Halo orbit and two corrections maneuvers approaching the asteroid. So it is assumed that few tens m/s are required to eventually correct the fly-by maneuver. Based on the previous consideration, a total ΔV of 400 m/s has been selected. Even though this value would not allow to reach all the targets listed in Table 6, it has to be remarked that the escape trajectory has not been optimized because it is outside the scope of this paper. Nevertheless, an optimized trajectory would decrease the required ΔV, composed of main and correction maneuvers.

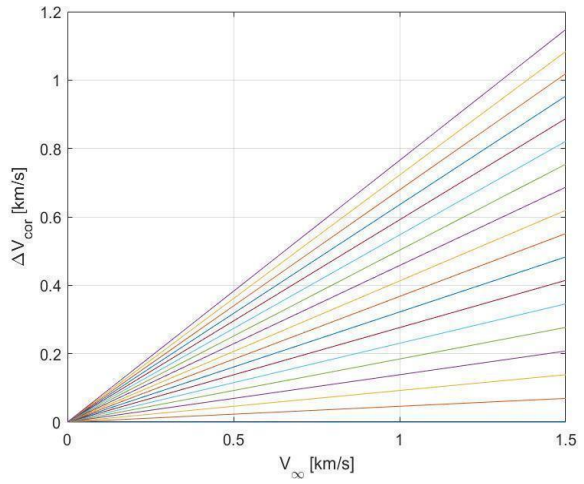

Figure 2: Correction ΔV for increasing correction angles

The high thrust maneuver require a chemical propulsion system. Table 7 reports the chemical COTS micro-propulsion systems that have been selected for the computation. Larger systems are also available on the market, but they do not fit this application in terms of mass and volume.

Using the Tsiolkovsky equation it is then possible to compute the relationship between propellant mass, CubeSat total mass, specific impulse and ΔV. Figure 3 reports this relation for increasing values of the CubeSat BOL mass (1-12 kg) and locates the available COTS thrusters. Following the philosophy of a light and compact 3U CubeSat, the plot shows that the best choice for this particular application is the Aerojet Rocketdyne MPS-130 1U, which would allow almost 4kg of CubeSat BOL mass and 2U for the other subsystems. MPS-120 1U has higher performances, but its propellant is hydrazine, which complicates the use of the CubeSat as a secondary payload onboard the launcher. Another valid option is the VACCO Argomoon Hybrid MiPS due to its 4 cold gas thrusters that can also be used for reaction wheel desaturation maneuvers, but it allows less CubeSat BOL mass.

Table 7: COTS chemical Micro-propulsion systems

Producer	Product	Max Thrust [mN]	Isp [s]	Dry-wet mass [kg]	Volume
Aerojet Rocketdyne	MPS-130[28]	1250	206-235	1.06, 1.66	1U
				1.36, 2.76	2U
Aerojet Rocketdyne	MPS-120[29]	1250	206-217	1.06, 1.48	1U
				1.36, 2.38	2U
VACCO	Green MiPS[30]	400	~190	3.0 5.0	3U
VACCO	Argomoon hybrid MiPS[31]	100+ 4x25	190	1.43 2.06	1.3U
NanoAvionics	EPSS C1[32]	1000 (BOL)	213	1,1.2	1.3U
Thethers Unlimited	HYDROS-C[33]	1200	>310	1.87,2.61	~2.5U
Hyperion Technologies	PM200[34]	500	285	1.1, 1.41	1U
Hyperion Technologies	PM400[35]	1000	285	1.4, 2.025	2U

The choice of a mono-propellant thruster is also justified by the burning time. Before injecting the CubeSat on the escape hyperbola, it is wise to fractionate the ΔV over various apogee raising maneuvers performed at the perigee. However, fractionating the transfer excessively leads to longer mission duration, which has to be taken into account for both the life of the components and for the radiation dose inside the Van Allen belts. For this reason, a mono-propellant engine is better suited for the application due to its larger maximum firing time. Liquid bi-propellant engines can generally fire continuously for

less time due to thermal issues related to the actual combustion. But their higher specific impulse would makes them more performant for other applications such as station keeping around an asteroid. A popular mission concept that has been explored and proposed previously, is a mothercraft carrying on-board multiple CubeSats, released in the close proximity of the targets. In this framework, Hyperion Technologies PM200 represents a better solution for the 3U CubeSat and can be easily substitute in the 1U slot of the architecture proposed in this paper. Moreover, its thrust vector control makes it suitable also for reaction wheels desaturation maneuvers.

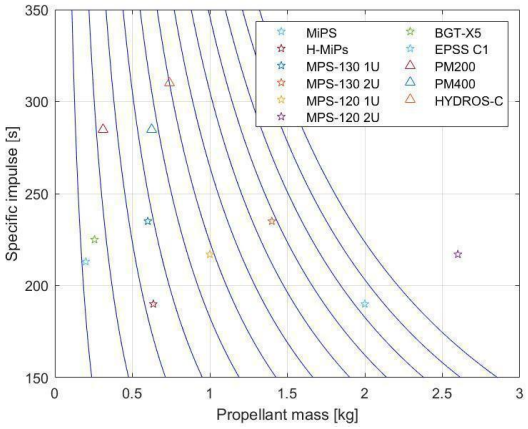

Figure 3: COTS Propulsion System evaluation chart; increasing BOL mass lines from left to right (1-12 kg)

STRUCTURE

Among the many, interesting solutions for a 3U CubeSat structure have been proposed by ISIS[36] (304 g) and by ENDUROSAT[37] (285 g). So, for mass budget an average 300 g will be considered. ISIS provides CubeSat structures up to 16U, while ENDUROSAT up to 6U, but the market is widely populated by other companies products in all sizes. However, an extensive structure analysis is outside the scope of this work, but for actual missions it is necessary.

POWER

The primary power is usually made available by solar panels. Many companies produce solar cells (AzurSpace, Emcore Corporation, Spectrolab, Solaero Technologies), which are assembled to form solar panels (AAC Clyde Space, DHV, Endurosat, GomSpace, ISIS, MMA Design LLC, NanoAvionics, Spectrolab). Solar cells efficiency is usually around 30%.[38]

There are many options feasible for 3U CubeSats, ranging from fixed panels to various configuration of deployable arrays. In order to increase the available on-board power, deep-space applications require deployable solar panels, such as used on MaRCO[1], Juventas[2], NEAScout[8], and INSPIRE[39].

Endurosat produces a 1-fixed 1-deployable solar panel configuration for a 3U CubeSat[40]. Each panel contains up to 7 Triple Junction Solar Cells InGaP/GaAs/Ge for a total of 14. The total weight, below 300 g, of a single panel does not fit with this application. ISIS offers a similar configuration made of GaAs solar cells, each 3U panel characterized by around 150 g of mass and 6.9 W of delivered power[41]. NanoAvionics produces deployable solar panels configuration characterized by 36.95 mW/cm^2 power-generation capacity in LEO[42].

Another type of deployable configuration is offered by both GomSpace and DHV technologies (together with Spire Global), characterized by double deployable solar arrays (135° version). The configuration of two near faces is characterized by a total of 2 fixed panels and 4 deployable ones. GomSpace configuration[43] has a total of 36 GaInP/GaAs/Ge solar cells, 30.18 cm^2 effective area each, giving up to 1.15 W per cell in LEO. DHV configuration[44] is characterized instead by 42 triple junction GaAs solar cells giving around 29.6W at 1AU for a total mass of 410 g. The problems related to this configuration are the limited power generation of the fixed solar cells and the limited orientation of the panels.

MMA design LLC configurations overcome these problems by means of totally deployable solar panels. Four slightly different HaWK configurations[45] (17A-42, 17AB36, 17AS42, 17AS56) are available, ranging from 42 to 56 solar cells, and from 36 to 56 W of power generation in LEO. HaWK 17AB36 configuration was installed on MarCO and its orientability, together with its weight (375 g excluding the deployment mechanism) makes it a valid candidate for many other deep-space application, as this one. Other deployable configurations have been designed by GomSpace for Juventas and M-Argo[46].

MMA Design LLC uses Spectrolab XTJ Prime solar cells[38], characterized by 30.7% BOL efficiency and 26 cm^2 area. After 10 years in LEO, the efficiency is decreased by a factor 0.94, so this value has been considered for further considerations[47]. Figure 4 shows the relation between distance from the Sun expressed in AU and the available on-board power for various incidence angles. The maximum distance to the Sun given in the plot compares to the maximum apogee of the asteroids given in Table 6.

The plot shows that up to 60 degrees incidence angle and in the farer scenario, the solar panels are still able to deliver more than 10 W to the CubeSat for its operation phase. However, as it will be discussed in the

Communication section, X-Band transmitters usually require slightly more than 10 W. Then, the use of orientable solar arrays plays again a fundamental role to reduce the incidence angle and further increase the available power.

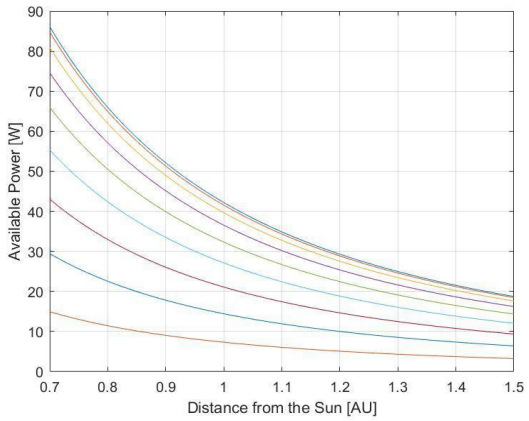

Figure 4: AU Sun distance vs Available power, incidence angles from 0° (top) to 80° (bottom)

The market offers a wide range of integrated battery and Electrical Power System (EPS) options. Table 8 reports the most promising integrated solution, but the available COTS components, especially batteries, are not limited to the table.

Table 8: COTS EPS

Producer	Product	Mass [g]	Volume [mm]	Battery Capacity [Wh]	Power Consumption [mW]
Endurosat	EPS I[48]	208	90.2x95.9 x21.2	10.2	75
Endurosat	EPS I Plus[48]	292	90.2x95.9 x30	20.4	75
GomSpace	NanoPower P31u[49]	200	89.3x92.9 x25.6	19.5	160
GomSpace	NanoPower P31u+BP4[49]	100+ 258	89.3x92.9 x15.3+94 x84x23	38.5	160
ISIS	iEPS-A[50]	184	96x92x26 .45	22.5	N/A
ISIS	iEPS-B[50]	310	96 x 92 x 11.34 +94.4 x 89.3 x 21	45	N/A
ISIS	iEPS-C[50]	360	96 x 92 x 15.95 +94.4 x 89.3 x 21	45	N/A
NanoAvionics	EPS[51]	N/A	N/A	N/A	150

To determine the requirement for the battery system, a sample maximum power load is taken from the average power consumption data of other subsystems. It is calculated that the power load is around 20W when all subsystems are active. As there are few eclipses expected during the mission lifetime a relative low number of duty cycles (charge and discharge) are expected. This means that the depth-of-discharge (DOD, the percentage of the battery that is discharged) can be high, as higher DOD decrease the number of duty cycles the battery can have. A DOD of 60% and battery efficiency of 0.9[101] is taken as representative values. The required battery capacity can then be calculated as follows:

$$C = \frac{P \cdot T}{DOD \cdot \eta} \quad (2)$$

where C is the capacity, P the power load, T the time without power (taken here to be around 30 minutes as an estimate), and η the battery efficiency. The required capacity then becomes: 18.51 Wh.

ATTITUDE DETERMINATION AND CONTROL

The ADCS is a combination of several sensor to determine the state of the spacecraft (e.g. Sun sensors, star trackers, hall-sensors, etc.), and actuators to control the orientation of the satellite (e.g. reaction wheels, thrusters). Many companies offer integrated ADCS solutions with all necessary sensors and actuators available, including processors capable of doing most of the computations needed for controlling the satellite. Thus these integrated solution will be the first focus for the ADCS selection. In terms of functionality and performance for the example mission discussed in this paper, there are two main parameters that influence the selection of the ADCS:

- The pointing accuracy: the degree of accuracy with which the ADCS can point the satellite in a specific direction.
- Actuator saturation/lifetime: the actuators used in the ADCS have specific constraints. For reaction wheels, there is a maximum amount of RPM that can be reached. And for a thruster solution there is a maximum amount of propellant on-board.

The pointing accuracy is mainly determined by three factors: the FOV of the payload, the directional accuracy required for thrusting maneuvers, and the maximum amount of pointing losses allowed for downlinking data. For the thrusting maneuvers accuracy no specific value is calculated as it is assumed that the other factors have stricter requirements, thus the thrusting accuracy will not be calculated. It is noted here that factors like jitter and agility are also important for the performance of the

payload and communication subsystem. However, as this data is not readily available in most cases, the pointing accuracy will be taken as the major selection criterium.

For the actuators it is important that there is a relatively large amount of momentum storage in the reaction wheel, or a large amount of propellant in case of reaction thrusters, and/or that there is a solution to desaturate the wheels. For most LEO satellites this is done using magnetorquers[52]. However, in deep-space, during large parts of the mission, the magnetic field is absent or too small. Moreover, other planets magnetic fields are known with a lower accuracy than the Earth's one. Therefore, magnetotorquers applicability for wheels desaturation is limited. For most deep space applications, this problem is solved using reaction thrusters that provide a counter torque during momentum dumping. There are only a few options for CubeSats in terms of reaction thrusters. One is the Aurora Propulsion Technologies AOCS[60], a water-based resistojet. Due to its chemical-free risk and its 12 thrusters, it is able to properly control and desaturate the CubeSat. However, also in this case, the minimum volume and mass configuration (10cm x 10 cm x 3 cm, 0.35 kg of wet mass) increases the complexity of the design. Another option is the VACCO MiPS cold gas propulsion system, which can be used for both translational and attitude maneuvers. which is similar in size but only contains 5 thrusters which can be used for all 6 DOF.

The minimum FOV for the payloads discussed and selected in the Scientific Instruments section is found for the Argus 2000 IR spectrometer: 0.15 degrees. In terms of pointing losses for communication, a previous study[53] determined that for deep space communication in the X-band frequency range, a maximum of 0.5 degrees pointing accuracy is acceptable. These two numbers will drive the selection of the ADCS subsystem, discussed hereafter.

The systems reported in Table 9 represent the most attractive solutions for a 3U CubeSat available on the market. XACT-15 would represent the best option for a standard CubeSat, due to its fine declared pointing accuracy and its flight heritage, but its large mass combined with the 0.5 U volume lower its applicability to this constrained mission. Instead, Hyperion Technologies iADCS-200 represents a more compact solution both in terms of volume and mass. A problem is that these systems have been designed for Earth's orbit environment and contain sensors and actuators not needed in deep-space (magnetometers, magnetorquers, Earth sensors). In terms of mass and volume, these extra instruments need to be removed. Whether it is cheaper to remove extra instruments rather than to integrate separated components remains questionable. Therefore, the current section reports also on individual actuators and sensors.

Table 9: Integrated ADCS

Producer	Product	Pointing accuracy (deg)	Volume [mm]	Mass [kg[	Nominal Power Consumption [W]
Hyperion Technologies	iADCS 200[54]	<<1	95 x 90 x 32	0.43	1.4
Blue Canyon Technologies	XACT-15[55]	0.003 (1σ)	100 x 100 x 50	0.885	N/A
KU Leuven	ADCS[56]	0.11	100 x 100 x 50	0.715	1.4
CubeSpace	3-axis ADCS + CubeStar[57]	0.2 (3σ)	90 x 96 x 52	0.328	0.57
Adcole Maryland Aerospace	MAI-500[58]	0.1 (LVLH) 0.008 (ECI)	100 x 100 x 62.3	1.049	1.82 (Min)

NanoAvionics 4RW0[59] represents an excellent control system for deep-space applications. It is composed by 4 reaction wheels with large momentum capacity respect to the integrated solutions presented in Table 9. But, its large mass (665 g), volume (92.5 mm x 92.5 mm x 51.3 mm) and peak power consumption (6 W compared to 0.6 W of its steady state behavior), pose several challenges in its applicability to this mission scenario.

Star trackers (Table 10) and Sun sensors (Table 11) are needed for attitude determination, but, as it will be shown in the following section, also for navigation purposes. All of the integrated options presented in Table 9 contain a star tracker and space for allocation of multiple Sun sensors. Both star tracker and Sun sensor datasheets made available by companies worldwide present accuracy data based on different approaches (1-σ, 3-σ, RMS). Even though accuracy is usually the most important parameter for an attitude sensor selection, this compact application will require to look especially into mass and volume, power consumption and integration difficulty with the rest of the ADCS. In terms of mass, volume, accuracy and power consumption, the most promising star trackers are represented by Hyperion Technologies ST-200, KU Leuven mini star tracker, and OCE Technology PST-1. For Sun sensor, the most

promising solutions are Hyperion Technologies SS200, Solar MEMS Technologies nanoSSOC-A60, and Adcole Maryland Aerospace MAI- Sun sensor.

Table 10: COTS Star Trackers

Producer	Product	Cross Boresight accuracy (“)	Volume [mm]	Mass [kg]	Power Consumption [W]
Hyperion Technologies	ST200[61]	30 (3σ)	29 x 29 x 38.1	0.04	0.6
Hyperion Technologies	ST400[62]	10 (3σ)	53.8 x 53.8 x 90.5	0.28	0.7
Blue Canyon Technologies	Standard NST[63]	18	100 x 55 x 50	0.35	<1.5 (Peak)
Blue Canyon Technologies	Extended NST[64]	18	250 x 100 x 100	0.9	<1.4 (Peak)
Adcole Maryland Aerospace	MAI-SS[65]	5.7	55 x 65 x 70	0.282	1.5 2 (Lost-in-space)
KU Leuven	Mini Star Tracker[66]	20 (1σ)	20 x 20 x 40	N/A	<1
KU Leuven	Star Tracker[67]	2 (1σ)	95 x 50 x 45	0.25	<1
CubeSpace	CubeStar[68]	~55 (3σ)	50 x 35 x 55	0.055	<0.142 (average) <0.254 (peak)
TY-Space	NST-3[69]	5 (3σ)	50 x 50 x 50	<0.165	N/A
Space Inventor	Star-T3[70]	<5 (1σ)	60 x 60 x 88	0.35	1
Sinclair Interplanetary	ST-16RT2[71]	5	62 x 56 x 38	0.158	<0.5
OCE Technology	PST-1[72]	6 (1σ)	32 x 32 x 45	0.05	0.5
OCE Technology	NST-2[72]	3 (1σ)	50 x 50 x 52	0.13	1

Table 11: COTS Sun Sensors

Producer	Product	Accuracy (deg)	Volume [mm]	Mass [g]	Power Consumption [mW]
Hyperion Technologies	SS200[73]	<1	24 x 15 x 3.5	3	40
New Space Systems	NCSS-SA05[74]	0.5 (RMS)	33 x 11 x 6	<5	<10
New Space Systems	NFSS-411[74]	0.1 (RMS)	34 x 32 x 20	<35	<37.5 (average) 130 (peak)
Adcole Maryland Aerospace	MAI-Sun Sensor (CubeSat)[75]	N/A	27.94 x 17.14 x 2.03	3.5	5 (optional)
Adcole Maryland Aerospace	MAI-Sun Sensor (Small Sat)[75]	N/A	50.8 x 19.05 x 2.03	5.5	5 (optional)
Adcole Maryland Aerospace	Digital Sun Sensor[76]	0.1	96 x 94 x 53 + 190 x 127 x 53	300	N/A
Chang Guang Satellite	Digital Sun Sensor[77]	<0.5	48 x 36 x 21	40	<300
Solar MEMS Technologies	nanoSSOC-D60[78]	0.5 (3σ)	43 x 14 x 5.9	6.5	~100
Solar MEMS Technologies	nanoSSOC-A60[79]	0.5 (3σ)	27 x 14 x 5.9	4	~10
Antrix Corporation LTD	4PiSun Sensor[80]	5 (Null accuracy)	55 x 40 x 30	N/A	N/A
OCE Technology	SS Series array[81]	1	60 x 60 x 26	77	Passive
Bradford	Mini Fine Sun Sensor[82]	0.2 (3σ)	50 x 46 x 17	50	Passive
Lens R&D	BiSon64-ET[83]	0.5 (3σ)	N/A	<33	N/A
Lens R&D	BiSon64-ET-B[84]	0.5 (3σ)	N/A	<33	N/A

NAVIGATION

By the date of writing, the only two deep-space CubeSats (MarCO-A and MarCO-B) were carrying on-board NASA-JPL Iris transponder[85], which allowed to perform deep-space tracking via X-Band tracking. The same architecture has been designed for many other planned deep-space CubeSats. Moreover, the successful communications with MarCO around Mars orbit proved the feasibility of communicating with a CubeSat at a large distance. However, Iris large mass and volume, coupled with the need of reducing ground tracking for future missions, trigger the selection of an autonomous optical navigation system. This would decrease both the ground tracking need and the mass and volume, due to the usability of the already on-board instruments (Payload Camera, Star trackers and Sun sensors) for navigation purposes during all the various phases of the mission, from relative navigation around the target body[86] to absolute navigation during deep-space cruise[87]. Especially for the cruise phase, it has been shown that celestial navigation offers an accuracy comparable to standard deep-space tracking[87]. The pure navigation design is left for future works, but it is assumed that star tracker, Sun sensors and payload camera (eventually used as NAVcam) will alse be used for navigation purposes.

COMMUNICATION

Deep-space communications usually rely on X or Ka Band frequency ranges. Due to the few available options for the latter option, this paper focuses on X-Band communication systems. As it has been mentioned in the payload section, laser communication technologies are continuously improving and their use for deep-space application cannot be excluded in the near future.

This application, which does not require uplink and tracking, can be accomplished by means of X-band transmitter and antennas.

A wide range of X-Band transmitters and antennas for CubeSat is offered by Syrlinks[99]: EWC27, N-XONOS, SPAN-X-T2 and SPAN-X-T3. However their datasheets are not available and they are not included in Table 12 and Table 13.

MarCO deployable reflectarray[100] has not been included in the tables because, despite the small storage volume (~0.1 U) and high gain (~29 dBi), its large mass (~1 kg) does not match with the strict requirements of this mission. However, even if it is not a proper COTS component (as Iris), it represents a really valuable solution for larger CubeSat architectures.

Table 12: X-Band Transmitter

Producer	Product	Transmitting power [W]	Volume [mm]	Mass [kg[	Power Consumption [W]
Endurosat	X-Band Transmitter[88]	2	90.2 x 95.9 x 23.6	0.27	12
AAC Clyde Space	Pulsar-Data[89]	2	96 x 90 x 11.7	0.13	< 1 5
Tethers Unlimited	SWIFT-XTX[90]	1-7	86 x 86 x 50	< 0.5	3 + (24-42)
Glavkosmos	X-Band Transmitter[91]	2.5	87 x 93 x 28	0.38	16
InnoFlight	SCR-106[92]	2.5	82 x 82 x 25	0.25	5 (average) 30 (peak)
Sputnix	X-Band Transmitter[93]	1	89 x 93 x 27	0.195	15
Space-SI	X-Band Transmitter[94]	1-2	N/A	0.5	10

Table 13: X-Band Antenna

Producer	Product	Gain [dBi]	Volume [mm]	Mass [g]
Endurosat	X-Band Patch antenna[95]	6	24 x 24 x 6.39	2.2
Endurosat	2 x 2 X-Band Patch antenna[95]	12	60 x 60 x 7.28	23.15
Endurosat	4 x 4 X-Band Patch antenna[95]	16	82.6 x 98 x 7.23	52.85
AAC Clyde Space	Pulsar-XANT[96]	7.75	36 x 36 x 4.7	< 10
AAC Clyde Space	Pulsar-XANT Plus[96]	11.5	58 x 58 x 4.7	< 29
Antenna Development Corporation*	11 dB Gain Unit[97]	10	6.35 x 63.5 x 66.6	53
Antenna Development Corporation*	16 dB Gain Unit[98]	16	8 x 150 x 104.1	300

*Antenna Development Corporation has been purchased by Blue Canyon Technologies (20 Dec. 2019).

Telecommunications link budget strongly depends on several factors. Deep-space required Eb/N0 is usually

1dB while the required link margin is 3dB[101]. Fig. 5 and Fig. 6 show the highest data rate for some proposed antenna architectures in function of the distance from the Earth. The ground antenna considered is 34-m diameter and standard losses have been considered, including pointing from the ADCS.

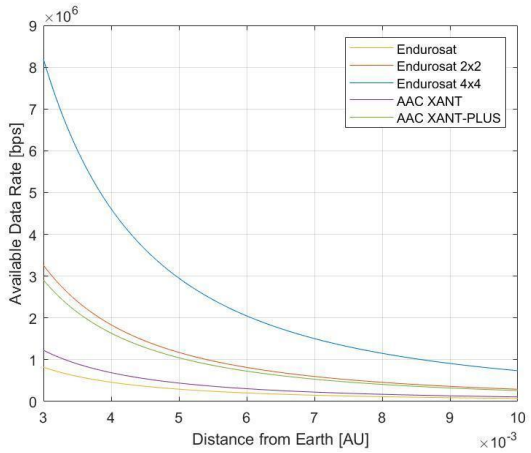

Figure 5: Available data rate in standard conditions

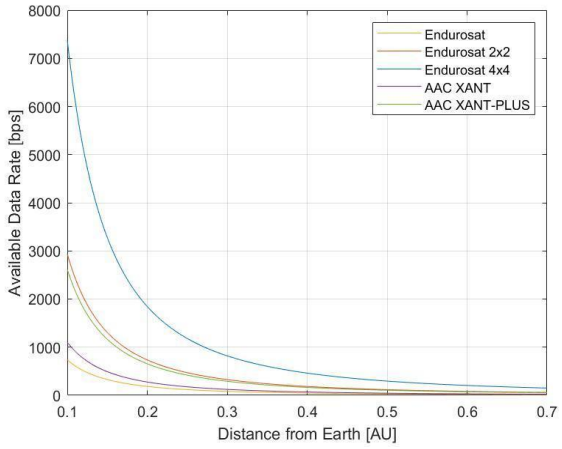

Figure 6: Available data rate in standard conditions

ON-BOARD DATA HANDLING

Depending on the configuration of the satellite, the on-board computer (OBC) can have many functions. For the mission discussed in this paper, functions like attitude determination and control, and initial payload image processing are done on separate processors located inside those subsystems. Thus, it is assumed that the main functions of the central OBC is: housekeeping, data processing and storage, autonomous operations, and communication.

Specifications of COTS On-Board Computers available on the market are given in Table 14.

Table 14: On-Board Computer

Producer	Product	Maximum clock frequency [Mhz]	Volume [mm]	Mass [g]	Power Consumption [mW]	Memory Storage [Gb]
Endurosat	OBC [102]	216	89 x 95 x 23.2	58	~340	0.256
AAC Clyde Space	KRYTEN-M3 [103]	50	95.89 x 90.17 x 23.24	61.9	400	0.008
AAC Clyde Space	Sirius OBC LEO N3FT [104]	50	95.89 x 90.17 x 17.20	130	1300	2
AAC Clyde Space	Sirius TCM LEO N3FT [105]	50	95.89 x 90.17 x 17.20	134	1300	32
Inno Flight	CF-300 [106]	767	92 x 89 x 14	< 120	1000 - 4000	16 (option to expand to 384)
Hyperion Technologies	CP400.85 [107]	500	50 x 20 x 10	7	550	7.5 to 64 (optional)
NanoAvionics	SatBus 3C2 [108]	400	N/A	N/A	N/A	0.256
GomSPace	NanoMind A3200 [109]	64	65 x 40 x 7.1	24	170	~0.160
Sat Revolution	Advanced OBC [110]	216	96 x 96 x 8	52	~1000	0.008
Sat Revolution	Basic OBC plus IMU [110]	16	96 x 96 x 8	37	N/A	N/A
Space Inventor	OBC – P3 [111]	300	N/A	N/A	N/A	0.128
ISIS	iOBC [112]	400	96 x 90 x 12.4	100	400	4 (optional 32)

There are several key factors that determine if a specific OBC is compatible with the mission or not. Important factors like the specific available peripherals and types of storage can be of importance when looking at compatibility with other subsystems. However, for the scope of this paper, this will not be considered. Instead, the focus will mainly be on: power usage, volume, mass, clock frequency, and data storage. Power, mass, and volume are obvious factors due to the 3U design constraint. The clock frequency of the processor in the OBC is of importance as it determines how many computations can be done per second. This (together with other factors like word size) determines what functions are possible to have on the OBC. Especially due to the required autonomy, the navigational aspects of the mission, together with the data processing, results in relatively high computational requirements. Next to the clock frequency, the data storage capabilities are also important due to the fact that during the fly-by there is no option to downlink the data at the same time. Thus, to increase the scientific output of the mission, a large amount of data needs to be stored on-board during this critical phase.

The low power usage of the Endurosat OBC, KRYTEN-M3, CP400.85, NanoMind A3200, and the ISIS iOBC are immediate advantages over other options. Combining this with good data storage capabilities and high clock frequencies, the CP400.85 and ISIS iOBC remain as two of the most promising options.

The Payload section highlighted two main instruments, Hyperion Technologies IM200 and Thoth Argus 200, that can be used to define the required OBC memory to store data. Data can be either downlinked during the scientific phase or after it; this second option clearly requires on-board storage and looks more promising for a low resource CubeSat. On-board stored data will be VIS images from IM200, IR data from Argus200 and navigation data from the autonomous GNC system. IM200 data acquisition can be computed around 22MB/s, while Argus200 is approximately around 6 KB/s and navigation data are negligible in size. This means that the required on-board memory is triggered by IM200 output, and, for example, Hyperion Technologies CP400.85 offers up to 48 minutes of scientific phase thanks to the 64 GB optional memory.

THERMAL

All of the COTS components datasheets present the operative temperature ranges. Generally operative temperature ranges are wide, but in few cases they can be small, such as for SCS Space Gecko Imager (10-30 °C). Nevertheless, the vast majority of COTS components is operative at least in the range -20,40 °C, reaching really large temperature intervals in many cases, such as for Lens R&D Sun sensors (-120,120 °C). A pure thermal control design is outside the scope of this paper; however, this section is devoted to briefly introduce the options already available on the market.

Thermal control is often a challenge for spacecrafts, especially for CubeSats or small satellites. The components mentioned in the previous sections present variable temperature operative ranges, depending both on the components and the manufacturer.

MarCO thermal control system was both active and passive, by means of radiators, blankets, heaters and various temperature sensors. INSPIRE and NEA Scout will encounter a less varying thermal environment and their thermal control systems are less challenging since they are around 1AU from the Sun[12]. However, thermal dissipation devices are needed especially for thrusters and batteries. The application analyzed in this paper may require similar constraints to INSPIRE and NEA Scout.

The market offers a good range of passive and active solutions for CubeSat thermal control. Multi-Layers Insulation (MLI) have been widely used for space applications and many companies offers solutions: Sheldahl, Dunmore, Aerospace, Fabrication and Materials, MLI Concepts inc.. In particular the Dunmore Aerospace Satkit including standard STARcrest materials, is optimized for small satellites and CubeSats, and it represents an excellent solution for deep-space CubeSats. Deployable radiators are currently produced by Thermal Management Technologies, and Kaneka Corporation together with JAXA proposed another excellent solution. Coatings (paint and tape) are offered by a wide range of companies: AZ Technology, MAP, Astral Technology Unlimited, Inc., Lord Techmark, Inc., Sheldahl, Akzo Nobel Aerospace Coatings. Sierra Lobo has developed a Sun shield, applicable to a 3U CubeSat (CryoCube), interesting in case of cryogenic experiments, but not needed in this application. A large number of flexible thermal straps, to allow passive thermal transfer to heat sink, in various materials: copper or aluminum by Thermal Management Technologies, K-Technology by Thermacore, Graphite Fiber by Technology Applications Inc.. Heat pipes for small satellites are offered by Advanced Cooling Technologies, Orbital ATK and Thermocoax. [38]

Concerning active thermal control, electric heaters are offered by Minco Products Inc. and All Flex Flexible Circuits LLC, while mini cryocoolers by Ricor-USA Inc., Creare, Sunpower Inc, Northrop Grumman and Lockheed Martin. [38]

RADIATION

Radiation may affect the CubeSat operations in two ways: Total Ionizing Dose (TID) and Single Event Effects (SEE). Many companies in the component datasheets claim their radiation tolerance. However few

datasheets present information on the TID, so it is difficult to compare the performances among them. The few data available show a minimum TID tolerance around 10 krad, with peak up to 70 krad.

Van Allen belt and solar particle flux may affect strongly the TID. For LISA pathfinder, a 100 krad TID has been computed around Sun-Earth Lagrangian points, while for a 3U CubeSat fly-bying an asteroid from the same point for 150 days, it has been computed a 10-20 krad TID with 0.5-1 mm thickness of aluminum shielding. [12] A proper radiation protection scheme needs to be designed for each application.

TRADE-OFF AND CONFIGURATION

Following the concepts highlighted in the previous sections, a CubeSat configuration is proposed, presenting trade-offs for components selection. Payload trade-off is not presented, because HT IM200 represents the only solution satisfying the mass and volume requirements with a sufficient ground resolution (see Table 5). The same happens for the micro-propulsion system, as it has been discussed in the dedicated section, and for other components later described in this section.

Trade-offs are based on an Analytic Hierarchy Process (AHP) available for free in a Matlab environment[113]. In the AHP, each characterizing parameter, needed for a trade-off comparison, is related to the others in terms of importance for the selection. Once all the relations between parameters are defined, they are used to build a criteria matrix. Then, for each parameter, an alternatives matrix is generated, including the normalized parameter values of each component in the comparison. Finally, the components ranking is generated by multiplying the eigenvector of the criteria matrix by a matrix storing all the eigenvectors of the alternatives matrices.

The EPS trade-off is based on three parameters: mass, volume and battery capacity. For the AHP, mass and volume are considered 2 times as important as battery capacity, because all the COTS considered for the comparison meet the battery capacity requirement highlighted in the dedicated section (Endurosat EPS I has not been included). Moreover, mass and volume represent huge driving parameters for this compact architecture. Figure 7 reports the results of the AHP; GomSpace P31u and ISIS iEPS-A appear as the most valuable solutions for this application. The former is characterized by a slightly higher mass, and lower volume and battery capacity. Then for this work, the GomSpace P31u is selected, keeping in mind that the ISIS iEPS-A is an equally valuable alternative.

The integrated ADCS trade-off follows four parameters: mass, volume, pointing accuracy and power consumption. Mass and volume are also in this case the driving parameters and they are respectively 2 and 4 times as important as pointing accuracy and power consumption. The pointing accuracy is not the most important parameter because all the solutions considered for the AHP fulfill PR4 (CubeSpace 3-axis ADCS does not fulfill it and then it is not considered for the trade-off). Figure 8 shows the results of the AHP and it highlights the Hyperion Technologies iADCS-200 as the best solution for this application. BCT XACT-15 has a significantly higher accuracy, but its larger mass and volume lower its applicability.

The X-Band transmitter trade-off is based on four parameters: mass, volume, transmitting power and power consumption. Mass, volume and transmitting power are considered 2 times as important as the power consumption, which is considered slightly less important for the selection because a sufficient power input is guaranteed (see Power section). Figure 9 shows that the best solution is represented by the AAC ClydeSpace Pulsar-Data, followed by the InnoFlight X-Band transmitter. The former is lighter and more compact, even if it has a slightly lower transmitting power and larger power consumption.

The X-Band antenna trade-off is based on three parameters: mass, volume and antenna gain. This is the only case where mass and volume are not considered as the driving parameters, because, as Figure 5 and 6 show, the antenna gain is fundamental for data transmission. Moreover, all the antennas are characterized by low mass and volume (Antenna Development Corporation 16dB unit is the only exception). Then, antenna gain is considered 10 times as important as mass and volume. Figure 10 show that Endurosat 4x4 patch antennas array is the best solution (accordingly also to Figure 5 and 6).

The OBC trade-off is driven by five parameters: mass, volume, clock frequency, memory storage and power consumption. All the five parameters are considered equally important. Figure 11 shows that the best option for this application is represented by Hyperion Technologies CP400.85.

Other components selected for this application without an AHP are:

- Aurora Propulsion Technologies AOCS for wheels desaturation and AOCS redundancy. It has been preferred to the VACCO MiPS due to its lower mass and volume.
- Hyperion Technologies SS200 due to its easy integrability to the ADCS (Table 11 shows plenty options for Sun sensors).
- Thoth Technologies Argus200 since it is the only COTS IR spectrometer meeting the payload requirements.
- MMA Design LLC HaWK due to its deployable configuration.

Table 16 reports all the components selected for this application.

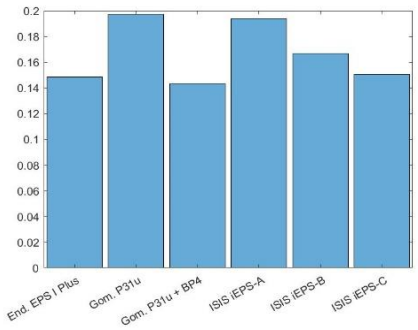

Figure 7: EPS Trade-Off

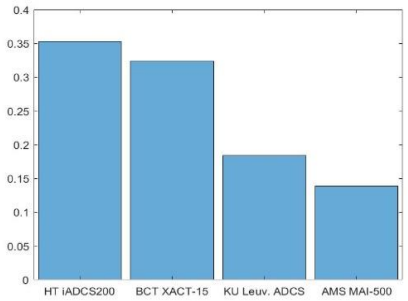

Figure 8: ADCS Trade-Off

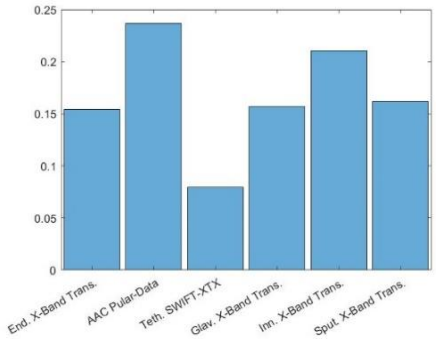

Figure 9: X-Band Transmitter Trade-Off

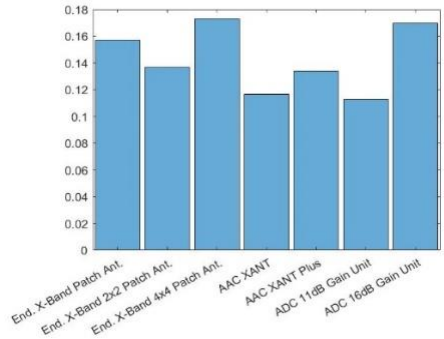

Figure 9: X-Band Antennas Trade-Off

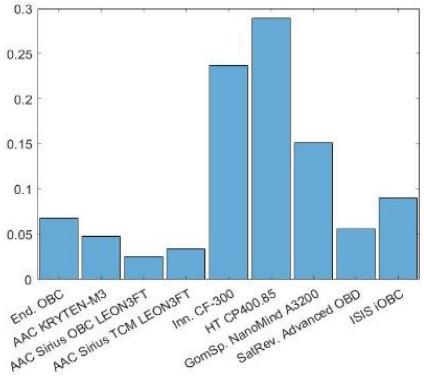

Figure 11: OBC Trade-Off

Table 16: Configuration

Component	Mass [g]	Volume
Endurosat Structure	285	3U
Aerojet Rocketdyne MPS-130	1700	1U
Hyperion Technologies IM200	59	~0.063 U
Thoth Technologies Argus200	300	~0.3U
GomSpace P31u	200	~0.18U
MMA Design LLC HaWK	375	1U x 3U x 7mm
Hyperion Technologies iADCS200	~300	0.3U
Aurora Technologies AOCS	350	0.3U
Hyperion Technologies SS200 (x6)	18	~0.007
AAC Clyde Space Pulsar-Data	130	~0.1U
Endurosat 4x4 Patch Antenna	53	~0.07U
Hyperion Technologies CP400.85	7	0.01U

Hyperion Technologies iADCS mass in Table 16 has been obtained by subtracting the weight of three magnetotorquers.

The total mass of the configuration proposed in Table 17 is below 3.8 kg and the 3U volume of the structure are enough to allocate all the components. Thermal passive control and radiation hardening are at this stage not

considered, but they should not add significant weight to the configuration. Moreover, power modes definition is required to ensure a correct sizing of the power system (Solar arrays, EPS and batteries), but due to the limited power demands of the components, it is fair to assume that the proposed power configuration is enough.

CONCLUSIONS AND FINAL REMARKS

The previous sections presented the advances of commercial-off-the-shelf small-satellite components for deep-space applications, evaluating their applicability and theoretical performances in a stand-alone CubeSat asteroid fly-by mission.

It has been highlighted that some subsystems are ready for deep-space and future applications, while other still need to overcome some issues. X-Band transmitters and antennas, on-board computers, electric power systems, solar arrays, attitude sensors (star tracker and Sun sensor) appear to be mature and performant for future deep-space applications. Moreover, the vast amount of choices, highlighted especially for Sun sensors, star trackers and OBCs, suggests the feasibility of many other applications (e.g. larger CubeSats, daughter-mother craft architectures).

On the other hand, micro-propulsion and ADCS sections highlighted that, despite the constantly increasing interest, they are not 100 % ready yet for this application. Only Aerojet Rocketdyne MPS-130 1U allows a sufficient mass and volume for other subsystems allocation, while larger applications (e.g. 6U) may be supported by more choices, such as Aerojet Rocketdyne MPS-130 2U or NanoAvionics EPSS C1. Another major drawbacks is reaction wheel desaturation, because it requires either multiple orientation thrusters or active thrust vector control, not available on the above mentioned systems. VACCO MiPS and Hyperion Technologies PM200 can orientate the thrust and desaturate the wheels, but their standard configuration in terms of propellant mass and specific impulse makes them more applicable to other scenarios, such as piggyback CubeSats or close-proximity release. It has been highlighted that the optimal solution for wheels desaturation, as of now, is to include another systems, such as the Aurora Propulsion Technologies AOCS, which complicates the overall architecture. Then, a monopropellant thruster, similar to Aerojet Rocketdyne MPS-130, with an integrated thrust vector control would be highly beneficial for this kind of applications. This work does not explore electrical and cold gas micro-propulsion systems, because the high thrust application presented here require chemical propulsion. Moreover, especially in the case of electric propulsion, it requires a low-thrust trajectory optimization which goes beyond the scope of this work. However, also these micro-propulsion systems saw a large improvement in the last years and their state-of-the-art is constantly updating. [114]

The cameras market is largely populated, even for larger applications, while other scientific instruments, IR spectrometers, laser altimeters or radars, are poorly or even not already available on the market. This is related to the strong dependence of the scientific payload on the particular application (more than other subsystems), but an increase of COTS scientific instruments, especially laser altimeters, would be beneficial for the near future space exploration with CubeSats.

Moreover, radiation hardening has to be carefully designed, because the vast majority of COTS components presented here are designed for LEO applications and shorter mission time.

The preliminary design of the proposed architecture shows the feasibility of COTS components application in deep-space, even if some limitations still need to be overcome.

As a final remark, data corresponding to specific components have been extracted from online available datasheets at the time of publication. For current more accurate values, interested readers should contact the specific vendors.

To conclude, approximately 40 companies have been mentioned in this paper, and many others were not included. This is a sign of how fast the small-satellite marketing is growing, considering that slightly more than 10 years ago, CubeSats were only considered for educational applications. This industrial growth, in coupling with the interest of scientific and academic community, will highly and beneficially influence the deep-space exploration of the next years, leading to a completely new mindset, driven by autonomous CubeSats.

ACKNOWLEDGEMENTS

This research is supported by the EU H2020 MSCA ITN Stardust-R, grant agreement 813644.

REFERENCES

1. Klesh, A.T., Baker, J. and J. Krajeswki, “MarCO: Flight Review and Lessons Learned,” Proceedings of the 33rd Annual AIAA/USU Conference on Small Satellites, Logan, UT, August 2019.
2. Goldberg, H.R., Karatekin, O. and B. Ritter, “The Juventas CubeSat in Support of ESA’s Hera Mission to the Asteroid Didymos,” Proceedings of the 33rd Annual AIAA/USU Conference on Small Satellites, Logan, UT, August 2019.
3. Michel, P., Küppers, M., Carnelli, I., “The Hera mission: European component of the ESA-NASA

AIDA mission to a binary asteroid," 42nd COSPAR Scientific Assembly, Pasadena, CA, July 2018.

4. Garner,. R., OSIRIS-REX, NASA, retrieved from https://www.nasa.gov/osiris-rex, accessed 4-5-2020.

5. JAXA, Asteroid Explorer Hayabusa 2, retrieved from http://www.hayabusa2.jaxa.jp/en/,, accessed 4-5-2020.

6. Granvik, M., Morbidelli, A., R. Jedicke et al., "Debiased orbit and absolute-magnitude distributions for near-Earth objects," Icarus, Volume 312, pp 181-207, September 2018.

7. Walker, R., Binns, D., C. Bramanti et al., "Deep-space CubeSats: thinking inside the box," Astronomy & Geophysics, Volume 59, Issue 5, October 2018.

8. McNutt, L., Johnson, L., P. Kahn et al., "Near-Earth Asteroid (NEA) Scout," Proceedings of the AIAA SPACE 2014 Conference and Exposition, San Diego, CA, August 2014.

9. Walker, R., Koschny, D., C. Bramanti et al., "Miniaturised Asteroid Remote Geophysical Observer (M-ARGO): A stand-alone deep space CubeSat system for low-cost science and exploration missions ," IPPW Small Sat Shoort Course, Boulder, CO, June 2018.

10. Speretta, S., Cervone, A., P. Sundaramoorthy et al., "LUMIO: An Autonomous CubeSat for Lunar Exploration," Space Operations: Inspiring Humankind's Future, pp 103-134, May 2019.

11. Kohout, T., Wahlund, J., T. Shimizu et al., "Asteroid prospection explorer (APEX) CubeSat for HERA mission," IPCS2019, 2019.

12. Machuca, P., Sanchez, J.P. and S. Greenland, "Asteroid flyby opportunities using semi-autonomous CubeSats: Mission design and science opportunities," Planetary and Space Science, Volume 165, pp 179-193, January 2019.

13. Hyperion Technologies IM200 datasheet, retrieved from https://hyperiontechnologies.nl/, accessed 26-5-2020.

14. Crystalspace Micro Camera System datasheet, retrieved from https://crystalspace.eu/, accessed 26-5-2020.

15. XCAM C3D datasheet, retrieved from http://www.xcam.co.uk/, accessed 26-5-2020.

16. SCS Space Gecko imager datasheet, retrieved from https://www.cubesatshop.com/product/scs-gecko-imager/, accessed 26-5-2020.

17. Hyperscout Cosine datasheet, retrieved from https://hyperscout.nl/, accessed 26-5-2020.

18. Simera-Sense datasheets, retrieved from https://simera-sense.com/, accessed 26-5-2020.

19. Thoth Argus2000 datasheet, retrieved from http://thothx.com/home, accessed 26-5-2020.

20. Carrasco-Casado, A., Biswas, A., R. Fields et al., "Optical Communication on CubeSats – Enabling the Next Era in Space Science," Proceedings of IEEE International Conference on Space Optical Systems and Applications, Okinawa, Japan, November 2017.

21. Hyperion Technologies Cubecat datasheet, retrieved from https://hyperiontechnologies.nl/, accessed 26-5-2020.

22. Hyperion Technologies MM200 datasheet, retrieved from https://hyperiontechnologies.nl/, accessed 26-5-2020.

23. Mani, K., Cervone, A. and F. Topputo, "Combined chemical-electric propulsion for a stand-alone mars CubeSat," Journal of Spacecraft and Rockets, Volume 56, N0. 6, December 2019.

24. Jaworski, S. and J. Kindracki, "Deployment of CubeSats from low-Earth orbit to Near-Earth Asteroids," 8th European Conference for Aeronautics and Aerospace Sciences (EUCASS), Madrid, Spain, July 2019.

25. Krejci, D., Gomez Jenkins, M. and P. Lozano, "Staging of electric propulsion systems: enabling an interplanetary CubeSat," Acta Astronautica, Volume 160, pp 175-182, July 2019.

26. JPL Small-Body Database Browser, retrieved from https://ssd.jpl.nasa.gov/sbdb.cgi, accessed 26-5-2020.

27. Machuca, P. and J.P. Sanchez, "Autonomous Navigation and Guidance for CubeSats to FlyBy Near-Earth Asteroid," Proceedings of the 70th International Astronautical Congress (IAC), October 2019.

28. Aerojet Rocketdyne MPS-130 datasheet, retrieved from https://www.rocket.com/, accessed 26-5-2020.

29. Aerojet Rocketdyne MPS-120 datasheet, retrieved from https://www.rocket.com/, accessed 26-5-2020.

30. VACCO MiPS datasheet, retrieved from https://www.cubesat-propulsion.com/, accessed 26-5-2020.

31. VACCO Argomoon MiPS datasheet, retrieved from https://www.cubesat-propulsion.com/, accessed 26-5-2020.

32. NanoAvionics EPSS C1 Datasheet, retrieved from https://nanoavionics.com/, accessed 26-5-2020.

33. Tethers Unlimited HYDROS-C datasheet, retrieved from https://www.tethers.com/, accessed 26-5-2020.

34. Hyperion Technologies PM200 datasheet, retrieved from https://hyperiontechnologies.nl/, accessed 26-5-2020.

35. Hyperion Technologies PM400 datasheet, retrieved from https://hyperiontechnologies.nl/, accessed 26-5-2020.

36. ISIS 3U CubeSat structure datasheet, retrieved from https://www.isispace.nl/, accessed 26-5-2020

37. ENDUROSAT 3U CubeSat Structure II datasheet, retrieved from https://www.endurosat.com/, accessed 24-4-2020.

38. NASA, "State of the Art Small Spacecraft Technology report", December 2018.

39. Klesh, A., Baker, J., J. Castillo-Rogez et al., "INSPIRE: Interplanetary NanoSpacecraft Pathfinder In Relevant Environment,", proceedings of the AIAA Space Forum, San Diego, CA, September 2013.

40. ENDUROSAT 3U Single deployable solar array datasheet, retrieved from https://www.endurosat.com/, accessed 24-4-2020.

41. ISIS 3U CubeSat solar panels datasheet, retrieved from https://www.isispace.nl/, accessed 26-5-2020.

42. NanoAvionics CubeSat GaAs Solar Panel datasheet, retrieved from https://nanoavionics.com/, accessed 26-5-2020.

43. GomSpace Deployable solar panels for 3U and 6U satellites 135 version datasheet, retrieved from https://gomspace.com/home.aspx, accessed 26-5-2020.

44. DHV Double deployable solar panels for 3U CubeSat datasheet, retrieved from http://dhvtechnology.com/, accessed 26-5-2020.

45. MMA HaWK datasheets, retrieved from https://mmadesignllc.com/, accessed 26-5-2020.

46. Goldberg, H.R., "Exploration in small packages: exploring asteroids with CubeSats", Stardust-R II Training School, Milan, Italy, February 2020.

47. Spectrolab 30. 7 % XTJ Prime Space Qualified Triple Junction Solar Cell datasheet, retrieved from https://www.spectrolab.com/index.html, accessed 26-5-2020.

48. ENDUROSAT EPS I datasheets, retrieved from https://www.endurosat.com/, accessed 24-4-2020.

49. GomSpace NanoPower P31u datasheets, retrieved from https://gomspace.com/home.aspx, accessed 26-5-2020.

50. ISIS iEPS datasheets, retrieved from https://www.isispace.nl/, accessed 26-5-2020.

51. NanoAvionics EPS datasheet, retrieved from https://nanoavionics.com/, accessed 26-5-2020.

52. Mazzini, L., "Flexible Spacecraft Dynamics, Control and Guidance," Springer, pp 101, 2016.

53. Van den Berg, M.L., Lyngvi, A.E. and P. Falkner, "Communication at large distances," Interstellar Heliopause Probe Technology Reference Study, April 2007.

54. Hyperion Technologies iADCS200 datasheet, retrieved from https://hyperiontechnologies.nl/, accessed 26-5-2020.

55. Blue Canyon Technologies XACT-15 datasheet, retrieved from https://bluecanyontech.com/, accessed 26-5-2020.

56. KU Leuven ADCS datasheet, retrieved from https://www.cubesatshop.com/, accessed 26-5-2020.

57. CubeSpace 3-axis ADCS datasheet, retrieved from https://www.cubespace.co.za/, accessed 26-5-2020.

58. Adcole Maryland Aerospace MAI-500 datasheet, retrieved from https://www.adcolemai.com/, accessed 26-5-2020.

59. NanoAvionics CubeSat Reaction Wheels Control System SatBus 4RW0 datasheet, retrieved from https://nanoavionics.com/, accessed 26-5-2020.

60. Aurora Propulsion Technologies AOCS datasheet, retrieved from https://www.aurorapt.fi/home/, accessed 26-5-2020.

61. Hyperion Technologies ST200 datasheet, retrieved from https://hyperiontechnologies.nl/, accessed 26-5-2020.

62. Hyperion Technologies ST400 datasheet, retrieved from https://hyperiontechnologies.nl/, accessed 26-5-2020.

63. Blue Canyon Technologies Standard NST datasheet, retrieved from https://bluecanyontech.com/, accessed 26-5-2020.

64. Blue Canyon Technologies Extended NST datasheet, retrieved from https://bluecanyontech.com/, accessed 26-5-2020.

65. Adcole Maryland Aerospace MAI-SS datasheet, retrieved from https://www.adcolemai.com/, accessed 26-5-2020.

66. KU Leuven mini Star tracker datasheet, retrieved from https://satsearch.co/, accessed 26-5-2020.

67. KU Leuven Star tracker datasheet, retrieved from https://www.cubesatshop.com/, accessed 26-5-2020.

68. CubeSpace CubeStar datasheet, retrieved from https://www.cubespace.co.za/, accessed 26-5-2020.

69. TY-Space NST-3 datasheet, retrieved from https://www.cubespace.co.za/, accessed 26-5-2020.

70. SpaceInventor STAR-T3 datasheet, retrieved from https://space-inventor.com/, accessed 26-5-2020.

71. Sinclair Interplanetary ST16RT2 datasheet, retrieved from http://www.sinclairinterplanetary.com/, accessed 26-5-2020.

72. OCE Technology Star trackers datasheet, retrieved from https://satsearch.co/, accessed 26-5-2020.

73. Hyperion Technologies SS200 datasheet, retrieved from https://hyperiontechnologies.nl/, accessed 26-5-2020.

74. NewSpace Systems Sun sensor datasheet, retrieved from http://www.newspacesystems.com/, accessed 26-5-2020.

75. Adcole Maryland Aerospace MAI Sun sensor datasheet, retrieved from https://www.adcolemai.com/, accessed 26-5-2020.

76. Adcole Maryland Aerospace Digital Sun sensor datasheet, retrieved from https://satsearch.co/, accessed 26-5-2020.

77. Chang Guang Satellite Digital Sun sensor datasheet, retrieved from https://www.cgsatellite.com/, accessed 26-5-2020.

78. Solar MEMS technologies nanoSSOC-D60 datasheet, retrieved http://www.solar-mems.com/, accessed 26-5-2020.

79. Solar MEMS technologies nanoSSOC-A60 datasheet, retrieved http://www.solar-mems.com/, accessed 26-5-2020.

80. Antrix Corportion LTD 4Pi Sun sensor datasheet, retrieved from https://satsearch.co/, accessed 26-5-2020.

81. OCE Technology Sun Sensor series datasheet, retrieved from https://satsearch.co/, accessed 26-5-2020.

82. Bradford space Mini fine Sun sensor datasheet, retrieved from https://www.bradford-space.com/index.php, accessed 26-5-2020.

83. Lens R&D BiSon64-ET datasheet, retrieved from https://lens-rnd.com/, accessed 26-5-2020.

84. Lens R&D BiSon64-ET-B datasheet, retrieved from https://lens-rnd.com/, accessed 26-5-2020.

85. Kobayashi, M.M., "Iris Deep-Space Transponder for SLS EM-1 CubeSat Missions," Proceedings of the 31st Annual AIAA/USU Conference on Small Satellites, Logan, UT, August 2017.

86. Franzese, V., Di Lizia, P. and F. Topputo, "Autonomous optical navigation for the lunar meteoroid impacts observer," Journal of Guidance, Control, and Dynamics, Volume 42, pp 1579-1586, July 2019.

87. Franzese, V. and F. Topputo, "Line-of-Sight Deep-Space Autonomous navigation," arXiv preprint arXiv:1909.08459, September 2019.

88. ENDUROSAT X-Band transmitter datasheet, retrieved from https://www.endurosat.com/, accessed 24-4-2020.

89. AAC Clyde Space Pulsar-Data datasheet, retrieved from https://www.aac-clyde.space/, accessed 26-5-2020.

90. Tethers Unlimited SWIFT-XTX datasheet, retrieved from https://www.tethers.com/, accessed 26-5-2020.

91. Glavkosmo CubeSat X-Band transmitter datasheet, retrieved from https://satsearch.co/, accessed 26-5-2020.

92. Innoflight SCR-106 datasheet, retrieved from https://satsearch.co/, accessed 26-5-2020.

93. Sputnix X-Band transmitter, retrieved from https://sputnix.ru/en/, accessed 26-5-2020.

94. Space-SI X-Band transmitter, retrieved from http://www.space.si/en/, accessed 26-5-2020.

95. ENDUROSAT X-Band antennas datasheets, retrieved from https://www.endurosat.com/, accessed 24-4-2020.

96. AAC Clyde Space Pulsar-Xant datasheets, retrieved from https://www.aac-clyde.space/, accessed 26-5-2020.

97. Antenna Development Corporation 11dBi X-Band antenna datasheet, retrieved from https://satsearch.co/, accessed 26-5-2020.

98. Antenna Development Corporation 16dBi X-Band antenna, retrieved from https://satsearch.co/, accessed 26-5-2020.

99. Syrlinks products, retrieved from https://www.syrlinks.com/, accessed 26-5-2020.

100. Hodges, R. E. , Chahat, N., Hoppe, D. J. and J. D. Vacchione, "A Deployable High-Gain Antenna Bound for Mars: Developing a new folded-panel reflectarray for the first CubeSat mission to Mars," IEEE Antennas and Propagation Magazine, vol. 59, no. 2, pp. 39-49, April 2017.

101. Wertz, J. R., Everett, D. F. and J. J. Puschell, "Space mission engineering: the new SMAD", Space technology library, 2011.

102. ENDUROSAT OBC datasheet, retrieved from https://www.endurosat.com/, accessed 24-4-2020.

103. AAC Clyde Space KRYTEN M3 datasheet, retrieved from https://www.aac-clyde.space/, accessed 26-5-2020.

104. AAC Clyde Space SIRIUS OBC LEON3FT datasheet, retrieved from https://www.aac-clyde.space/, accessed 26-5-2020.

105. AAC Clyde Space SIRIUS TCM LEON3FT datasheet, retrieved from https://www.aac-clyde.space/, accessed 26-5-2020.

106. Innoflight CF-300 datasheet, retrieved from https://satsearch.co/, accessed 26-5-2020.

107. Hyperion Technologies CP400.85 datasheet, retrieved from https://hyperiontechnologies.nl/, accessed 26-5-2020.

108. NanoAvionics SatBus 3C2 Datasheet, retrieved from https://nanoavionics.com/, accessed 26-5-2020.

109. GomSpace NanoMind A3200 datasheet, retrieved from https://gomspace.com/home.aspx, accessed 26-5-2020.

110. SatRevolution OBC datahseets, retrieved from https://cubesatworld.com/, accessed 26-5-2020.

111. SpaceInventor OBC-P3 datasheet, retrieved from https://space-inventor.com/, accessed 26-5-2020.

112. ISIS iOBC datasheet, retrieved from https://www.isispace.nl/, accessed 26-5-2020.

113. Rich, R., "ahp_simple()", retrieved from https://www.mathworks.com/matlabcentral/fileexchange/60647-ahp_simple, MATLAB Central File Exchange, accessed 26-5-2020.

114. Tummala, A. R. and A. Dutta, "An overview of Cube-Satellite propulsion technologies and trends;" Aerospace MDPI, December 2017.